Physics – Uspekhi **40** (11) 1163 – 1173 (1997)

PHYSICS OF OUR DAYS

PACS number: **52.90.+z**

Quasicrystalline structures in strongly coupled dusty plasma

A P Nefedov, O F Petrov, V E Fortov

Contents

Abstract. Dust particle ordering is discussed in various types of low-temperature plasma, such as thermal plasmas at atmospheric pressure, dc glow discharges, and UV-induced plasmas. Experimental data and numerical simulation results are presented. Properties of ordered structures are discussed and the conditions of formation considered.

1. Introduction

A plasma containing macroscopic particles or grains (often referred to as an aerosol or heterogeneous plasma, or plasma with a disperse condensed phase) has the feature that a particle introduced into such a plasma or produced in it by, say, condensation may be charged by an electron or ion flux or by photo- or thermoelectron emission [1 – 3]. Electron emission from a grain surface produces a positive charge, increases the electron density in the gas phase and hence enhances its electrical conductivity. Capturing electrons makes dust grains charged negatively, producing the reverse effect, a reduction in the electron density [4 – 7].

The distinguishing feature of a dusty plasma is that, owing to the relatively large size of a grain (from hundredths of a micron to tens of microns), its charge Z_p may assume extremely large values of up to $10^2 - 10^5$ electron charges. Therefore the (Z_p^2-dependent) Coulomb interaction energy of the grains may, on average, be much greater than the thermal energy, which makes the plasma strongly non-ideal [8]. Equilibrium calculations show that under certain conditions a strong intergrain correlation leads to a gas-liquid- solid phase transition and makes the grains arrange themselves into spatially ordered structures similar to those existing in liquids and solids [9]. (The electron and ion gases remain ideal analogous to those in a Debye plasma). Unlike an ordinary atomic liquid or a solid, dust grains are sufficiently large to scatter light considerably at even low volume fractions and may be detected individually by a video camera or other optical means. Quasicrystalline structures of dust grains have been observed for example, in a dc glow discharge in neon [10]. In Figure 1, a horizontal and vertical section of a dust cloud is shown.

Crystal-like structures that form in plasmas from low-thermal-energy, strongly electrostatically coupled charged grains have been analyzed theoretically by Ikezi [9] and have come to be known as Coulomb or plasma crystals.

One of the earliest observations of such quasicrystals involved charged micron-sized iron and aluminum particles held by a certain configuration of an alternating and a static electric field [11]. In later studies, Coulomb crystals of atomic ions were found in other types of traps, notably in the Penning trap [12], and then in a weakly ionized plasma in a radio-frequency discharge at low pressure [13 – 16]. In such a plasma, the degree of ionization is low ($\sim 10^{-7}$), the electron energy is a few electronvolts, and the ion energy is close to the thermal energy of the atoms (≈ 0.03 eV) [17]. The charge was usually formed in argon at a pressure of a few millibars between two planar horizontal electrodes to which a voltage with a frequency of approximately 14 MHz was applied. Because the electrons are more mobile and have a higher temperature than the ions, a large negative charge of the order of $10^4 - 10^5$ electron charges was acquired by the dust grains. The dust cloud was maintained in the space charge layer near the negatively charged electrode, where a balance of gravitational and electrostatic forces occurs [18]. This cloud was typically a disk a few centimeters in diameter, in which the number of particle layers running parallel to the electrode was several tens in the vertical direction, the average grain spacing being several hundred microns. As a result, the Coulomb

A P Nefedov, O F Petrov, V E Fortov High Energy Density Research Center, Russian Academy of Sciences
ul. Izhorskaya 13/19, 127412 Moscow, Russia
Tel./Fax (7-095) 485-79 90
E-mail: ipdustpl@redline.ru

Received 19 May 1997
Uspekhi Fizicheskikh Nauk **167** (11) 1215 – 1226 (1997)
Translated by E G Strel'chenko; edited by L V Semenova

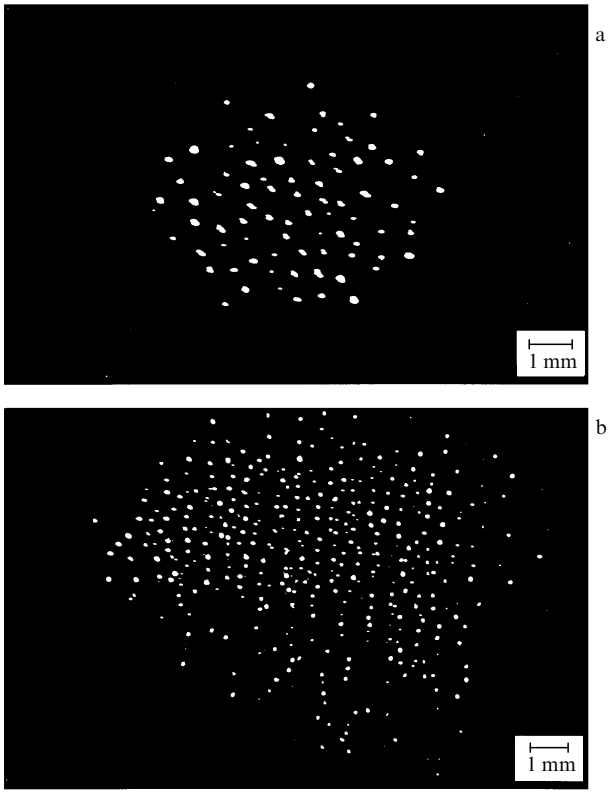

Figure 1. Video images of glass spheres in horizontal (a) and vertical (b) planes for a discharge current of 1.2 mA and a neon pressure of 0.2 Torr. Length scale 1 mm.

crystal was essentially two-dimensional (vertical layers outnumbering the horizontal ones by an order of magnitude), and its formation in the electrostatic trap involved the alignment of several thousands of regularly spaced particles. Note that the number of layers in the vertical plane is limited by gravitational forces and that the effect of these forces may be reduced by working under microgravitation conditions [19].

Thus, in practically all known experiments, ordered structures were observed either in a cloud of like charges or in a near-electrode space charge layer containing from hundreds to a few thousand charged grains. In either case the grain interaction potential, whose form strongly affects phase transitions in the plasma, may differ considerably from that in a classical quasineutral plasma. In the latter case, interacting particles are traditionally described either in terms of a one-component plasma (OCP) or by a screening (Debye) potential [8, 20–23] (also known as the Yukawa model).

These models consider classical, quasineutral, spatially confined plasmas for which the phase transition values of the grain coupling parameter $\gamma_p = (Z_p e)^2/\bar{r}kT_g$ have been obtained by numerical simulation [8, 9]. Here T_g is the plasma temperature, $\bar{r} = (4\pi n_p/3)^{-1/3}$ is the average intergrain spacing, and n_p the grain density.

An OCP is an idealized system of ions moving in a uniform neutralizing background, so that the system as a whole is electrically neutral. The interparticle potential $U(r)$ is a Coulomb one, and for γ_p in excess of $\gamma_c = 171$ [20] a regular crystal structure forms in a three-dimensional system. For low values of γ_p ($\gamma_p < 4$), the plasma is 'gas-like' [2, 8]. The Debye model considers the screening of charges by the background, which leads to the Debye-Huckel interaction potential [21–23]. To incorporate this screening, whose influence is determined by the ratio $\varkappa = \bar{r}/r_D$ (r_D being the Debye length), a parameter $\Gamma_s = (Z_p e)^2 \exp(-\bar{r}/r_D)/\bar{r}kT_g = \gamma_p \exp(-\bar{r}/r_D)$ is introduced. Thus, in the Debye model there are two parameters, γ_p and $\varkappa$, to describe the thermodynamics of the plasma and hence plasma phase transitions. The limiting cases of this model are the OCP model (for $\bar{r}/r_D \to 0$) and the hard spheres model (for $\bar{r}/r_D \to \infty$) [21].

Debye model calculations show that crystallization requires $\gamma_p \approx 99$ at $\varkappa = 0.7$, $160 < \gamma_p < 850$ at $1 < \varkappa < 5$, and $\gamma_p = 4.8 \times 10^4$ for $\varkappa = 10$ [21, 22], whereas dust grain systems in the RF-discharge boundary layer exhibit crystalline structures for $2.1 \times 10^4 < \gamma_p < 1.6 \times 10^5$ at $0.6 \leqslant \varkappa \leqslant 4.8$ [14] or for $\gamma_p \sim 10^6$ at $\varkappa \sim 9.8$ [16].

For plasmas held by traps, the phase state of the system is also affected by the boundary conditions as shown experimentally and by numerical simulation [24, 25]. For example, in a spherical trap the dust cloud is divided into spherical layers. Instead of sharp phase transitions, the system gradually evolves from the liquid state characterized by short-range order, through an intermediate state, in which a liquid coexists with a solid, and finally to a pure solid [25].

For plasma crystals under RF-discharge conditions, the liquid–crystal phase transition is also greatly affected by the two- dimensional nature of the crystal structure. Thus, instead of the first-order transition found in three dimensions, a two-stage transition was experimentally observed, with an intermediate state characterized by a short-range translational and long-range orientational order [19].

In parallel with the study of the properties of plasma crystals under RF-discharge conditions, in recent years attempts to obtain extended, essentially three-dimensional ordered structures in the bulk of a quasineutral plasma have been made, and structure formation processes for various charging mechanisms, particularly secondary emission and photoemission, have been investigated.

An example is the observation of macroscopically ordered structures in a bulk thermal plasma under quasineutrality conditions at atmospheric pressure and temperature of about 1700 K. The plasma studied was homogeneous, relatively large in size (its volume of 30 cm^3 corresponding to a particle number of the order 10^8 and particle density 10^7 cm^{-3}), and free of external electric and magnetic fields [26]. Owing to the large plasma volume and the availability of reliable plasma diagnostics techniques, various types of gas and particle measurements have been performed, plasma state parameters obtained and also comparisons with numerical simulation results has been made.

Three-dimensional quasicrystalline structures were obtained in the positive column of a dc glow discharge [27] with the quasineutrality condition obeyed to within 0.01% [28]. The analysis of grain images showed that the grains form a quasicrystalline structure in the horizontal plane while at the same time aligning in chains in the vertical plane. By varying plasma parameters, it was possible to change the dust cloud from an elliptic to cylindrical shape in the vertical plane, with structures typically a few centimeters across [10].

It has also been shown by a number of workers that on exposure to intense UV radiation dust grains may become positively charged and form crystalline structures, a fact of great promise for modeling the spatial ordering of particles in dust clouds in space [3].

2. Classical strongly coupled thermal plasma

The thermal plasma was produced from a neutral gas (heated to 1700–2200 K) at atmospheric pressure. The electrons, ions, and neutral particles had equal temperatures, and the electron densities were in the range $10^9 - 10^{12}$ cm^{-3}. The dust grains introduced into the plasma were charged by electron and ion fluxes (as is the case in a low pressure discharge) and by electron emission. In contrast to previous low pressure discharge experiments, which involved negative charges, thermal emission may charge dust grains positively. In the extreme case, grains placed in an ionized gas fully dominate the electrical and physical properties of the plasma. There is a wide range of conditions over which a plasma with dust grains can exist. Because the charge on a grain may be large (of order $10^2 - 10^3 e$), plasmas typically exhibit the entire range of states from a Debye plasma to a strongly non-ideal plasma, depending on the grain size and density, the work function, and the electron and ion densities [2].

Ordered structures in thermal plasmas were studied for the system of charged dust grains in a practically laminar weakly ionized flow at atmospheric pressure and a temperature of about two thousand degrees.

2.1 Experimental setup

The plasma source (a two-torch propane-air Mekker burner) produced a laminar plasma jet ($V_g = 2-3$ m s^{-1}, $T_g = 1700-2200$ K) with the pressure and temperature of electrons and ions uniformly distributed over the inner torch (25 mm in diameter and 70 mm in height, Fig. 1) at atmospheric pressure [26, 29–31]. Into the inner torch, CeO_2 particles were introduced. The choice of cerium dioxide as the grain material was due to its being chemically inert and because of the low work function (~ 2.75 eV [32]) of the CeO_2 grain surface. Due to the admixture of alkali compounds in the cerium dioxide powder, the presence in the plasma jet of potassium atoms with their low ionization potential of 5.14 eV was revealed by spectral measurements. Thus, the plasma source produced a rather extended and homogeneous volume (~ 30 cm^3) of quasineutral thermal plasma with positively charged CeO_2 grains suspended in it. Along with the grains, electrons and singly charged Na^+ ions were the basic plasma components.

The relatively large size and homogeneity of the plasma volume enabled various measurement techniques, both probe and optical, to be applied to the gas and the grains (Figs 2 and 3) and thus allowed the plasma state parameters to be determined. The density n_i of positive alkali ions was determined by the electric probe method [33, 34]. The technique for determining the local electron density n_e involved the measurement of the current I and the longitudinal electric field E in the plasma [30]. The gas temperature and the alkali metal concentration were measured in a traditional way using the generalized conversion method and the total absorption method [29]. To determine the average (Sauter) diameter D_p and dust density n_p in the plasma jet, an original laser technique was employed [34].

We note here that the spatial dust grain structures were studied by measuring the pair correlation function $g(r)$ that determines the probability for finding a particle at a certain distance from a given particle. The correlation function and the spatial arrangement of the particles were analyzed using a laser time-of-flight counter [30]. The measuring volume of the counter was formed by focusing the argon laser beam of

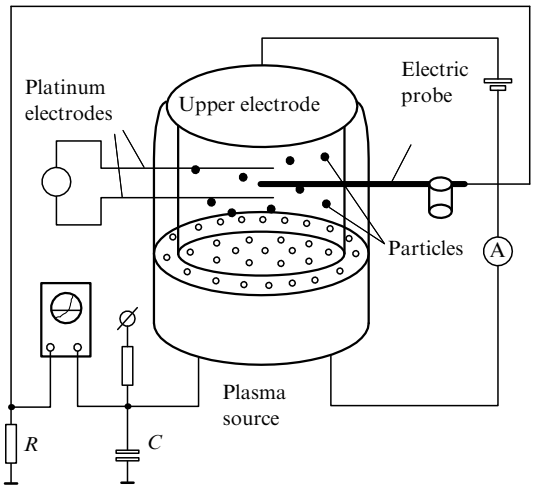

Figure 2. Thermal plasma source and probe diagnostic tools.

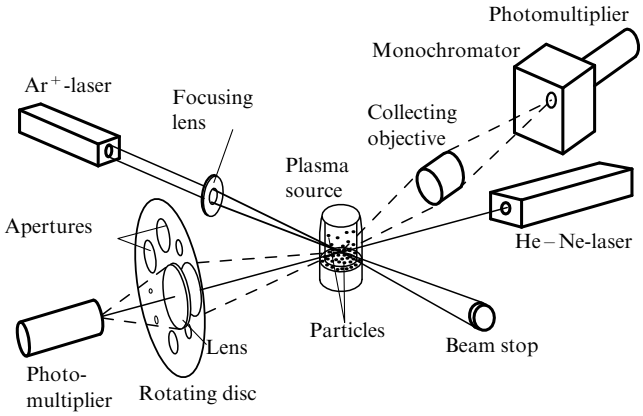

Figure 3. Schematic drawing of the instrumentation for measuring the size, density, and spatial structures of dust grains in a thermal plasma.

$\lambda = 0.488$ μm on a given portion of the plasma jet (Fig. 3). The pulses scattered from isolated grains were converted to electrical signals using a photomultiplier. The signals obtained were processed for calculating the correlation function $g(r)$, where $r = V_p t$. Here V_p is the mean dust grain velocity ($V_p \approx V_g$ for micron size particles) and t is the time.

Results on spatial grain macrostructures were compared with room temperature aerosol jet results for the case when only air with CeO_2 particles was supplied to the inner torch of the burner. Such a system models a plasma with a random spatial grain arrangement (a 'gas-like' plasma).

2.2 Spatially ordered structures in a bulk thermal plasma

Figure 4 shows typical pair correlation functions $g(r)$ for CeO_2 grains in an aerosol jet at room temperature ($T_g \approx 300$ K) and in a plasma ($T_g = 2170$ K and 1700 K). It is readily seen that the correlation function $g(r)$ for a plasma at $T_g = 2170$ K and grain density $n_p = 2.0 \times 10^6$ cm^{-3} is virtually the same as that for the aerosol jet, implying that grains interact weakly and the formation of ordered structures is not possible. This is also borne out by independent (probe and optical) plasma diagnostic measurements, from which the coupling parameter γ_p and the Debye screening

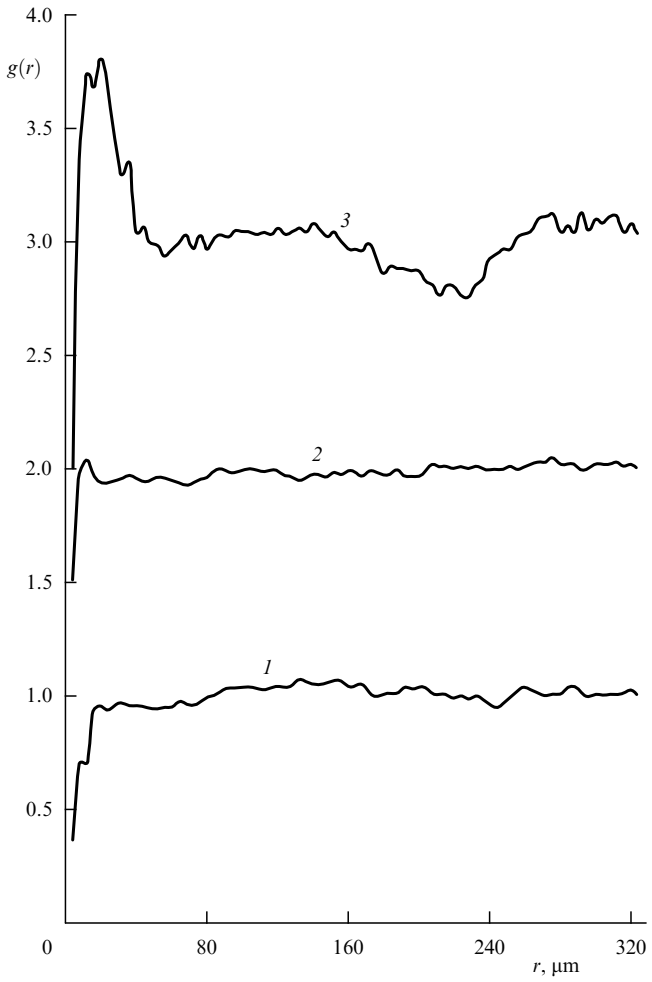

Figure 4. Pair correlation function $g(r)$ for CeO_2 particles in an air jet at room temperature $T_g \cong 300$, $\gamma_p = 0$ (*1*), and in a plasma ($Z_p = 500$): at a temperature $T_g = 2170$ K, $\gamma_p = 40$ ($\Gamma_s = 1$) (*2*) and at $T_g = 1700$ K, $\gamma_p = 120$ ($\Gamma_s = 40$) (*3*).

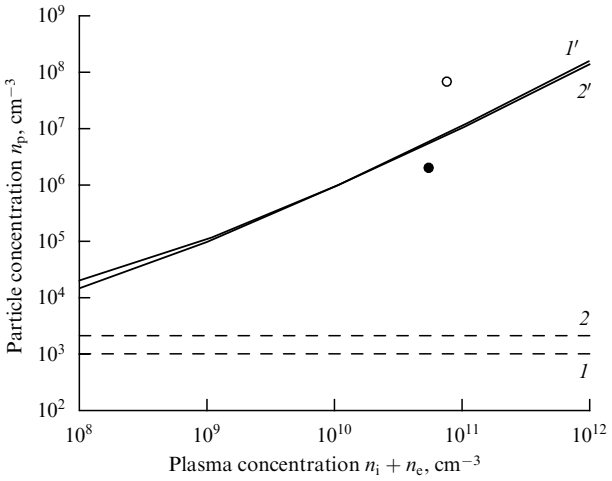

Figure 5. Plasma ($n_i + n_e$) and particle (n_p) density range within which an ordered structure forms at $Z_p = 500$. Curves *1*(*1′*) and *2* (*2′*) correspond to $\gamma_p = 4$ ($\Gamma_s = 4$) at $T_g = 1700$ K and 2200 K, respectively; $\gamma_p = 40$ ($\Gamma_s = 1$) (•) and $\gamma_p = 120$ ($\Gamma_s = 40$) (○) for a plasma with CeO_2 particles.

parameter $\varkappa = \bar{r}/r_D$ are calculated to be 40 and 3.5, respectively, and the parameter $\Gamma_s = \gamma_p \exp(-\varkappa) \approx 1$.

To analyse the experimental data let us consider the n_e and n_p range (see Fig. 5), in which ordered structures can form [36]. Curves *1* (*1′*) ($T_g = 1700$ K) and *2* (*2′*) ($T_g = 2200$) correspond to $\gamma_p = 4$ ($\Gamma_s = 4$). Short-range-ordered grain arrangement appears in the region above the curves *1*, *2* (OCP model) or *1′*, *2′* (Debye model). The Debye model predicts higher values of γ_p for the intergrain spacing and Debye length values obtained. The experimental point ($T_g = 2170$ K and $n_p = 2.0 \times 10^6$ cm^{-3}) marked by • in Fig. 5 [the corresponding correlation function is shown in Fig. 4 (curve *2*)] lies below the boundary between weakly and strongly nonideal plasma states — as it should according to the Debye model.

At a lower plasma temperature $T_g = 1700$ K and grain density $n_p = 5.0 \times 10^7$ cm^{-3}, it is seen from Fig. 4 (curve *3*) that the pair correlation function $g(r)$ displays the short-range order characteristic of a liquid. Under these conditions, diagnostic measurements showed the ion density ($n_i \sim 10^9$ cm^{-3}) to be about an order of magnitude lower than the electron density ($n_e \sim 10^{10}$ cm^{-3}). The grain charge as derived from the quasineutrality condition in the form $Z_p n_p = n_e, n_i \ll n_e$ had a positive value of about $10^3 e$ to within a factor of 2, the uncertainty presumably being due to the thermal emission of electrons from the grain surface [2, 30]. From diagnostic measurements, the parameters γ_p and $\varkappa$ were found to have the values of more than 120 and 1.6, respectively, which implies a gas-liquid phase transition according to the criterion of Ref. [2]. Thus, the grains form an ordered structure, which is consistent with the plasma state diagram of Fig. 5. The corresponding experimental point (○ in Fig. 5) lies above the theoretical curves for the Debye model.

Ordered structures were only observed to form at high dust grain densities ($\sim 10^7$ cm^{-3}). Reducing the CeO_2 density increases the average intergrain spacing and lowers the Coulomb interaction energy, thus preventing the formation of ordered structures as shown in Fig. 4 (curve *2*) ($n_p = 2.0 \times 10^6$ cm^{-3}).

2.3 Numerical simulation of ordered structure formation

To examine phase transitions in a particle system kept in a trap generally requires that external fields be considered and a particle interaction potential adequately chosen, which complicates numerical simulation so much that to date little progress has been achieved in this area. In thermal plasmas, where the relatively large volumes, homogeneity and the absence of external electric and magnetic fields reduce the effect of boundary conditions on phase transitions, it is expected the known — OCP or Debye — models are adequate for interpreting experimental data and that one can assess the validity of these models for describing plasma phase transitions. Such an analysis has been carried out [37] based on Monte Carlo simulations.

Calculations were made for a plasma with CeO_2 grains of density $n_p = 5.0 \times 10^7$ cm^{-3} at an electron density $n_e = 7.2 \times 10^{10}$ cm^{-3}, ion density $n_i = 0.42 \times 10^{10}$ cm^{-3}, and plasma temperature $T_g = 1700$ K. Under these conditions, the Debye length r_D and the average intergrain spacing $\bar{r}$ were 11 μm and 17 μm, respectively. Since the electron and ion densities are about three orders of magnitude higher than the dust density, it follows that plasma modeling calculations are only possible if one introduces an effective intergrain potential averaged over electron and ion positions. Note that the form of the effective potential has not yet been found,

although at present the Debye potential is considered to be the most reliable choice.

The nonideality parameter $\Gamma_p = (Z_p e)^2/kT_g r_D$ may be written in the form $\Gamma_p = \gamma_p \bar{r}/r_D$. Under experimental conditions, for $\bar{r} = 17$ μm and $r_D = 11$ μm, typically $\gamma_p \cong 120$, $\Gamma_p = \gamma_p \bar{r}/r_D \cong 185$ for $Z_p = 500$ and $T_g = 1700$ K.

An alternative model taken for analyzing and comparing the computed and experimental results was an OCP in which dust grains with the Coulomb interaction between them are immersed a uniform compensating background of the opposite charge. Since the OCP model has received detailed Monte Carlo study in the literature [8, 20], a comparison of the numerical results from both models seems appropriate. In doing this, it is important to note the similarity property of the OCP model, i.e. the fact that all results in it depend on a single dimensionless parameter γ_p; in the Debye model, two dimensionless parameters, γ_p and $\varkappa = \bar{r}/r_D$, determine the results. Debye model calculations were made for two values of $\varkappa = 1.0$, and 2.0, which correspond to the experimental conditions used and enable trends in the behavior of the calculated quantities to be analysed for comparison with the OCP results.

The starting point for the analysis of numerical results is to consider the pair correlation functions $g(r)$ of the one-component model. Figure 6 shows the dust grain functions $g(r)$ for γ_p values in the range 1 to 140 [8]. Note that crystallization within this model occurs at $\gamma_p = 171$ and that the pair correlation function $g(r)$ for $\gamma_p = 171$ satisfies the crystallization criteria mentioned above.

The results of the calculations of $g(r)$ for the Debye model at analogous Γ_p values are shown in Figs 7 and 8 for $\varkappa = 1$ and 2. From comparison and analysis of Figs 6–8 it is seen that as far as the function $g(r)$ is concerned, the Debye and OCP models come closest at $\varkappa = 1$ — as indeed they should because for $r_D \to \infty$ they become identical. For $\varkappa = 1$, increasing Γ_p to 1000 (which is much in excess of experimental values of Γ_p) causes no grain crystallization. This is seen by noting the crystallization criteria such as the ratio R_g of the minimum (g_{min}) to the maximum (g_{max}) value of the correlation function (in our experiment $R_g > 0.2$); and the behavior of the structural factor $S(q)$ [38] as shown in Fig. 9.

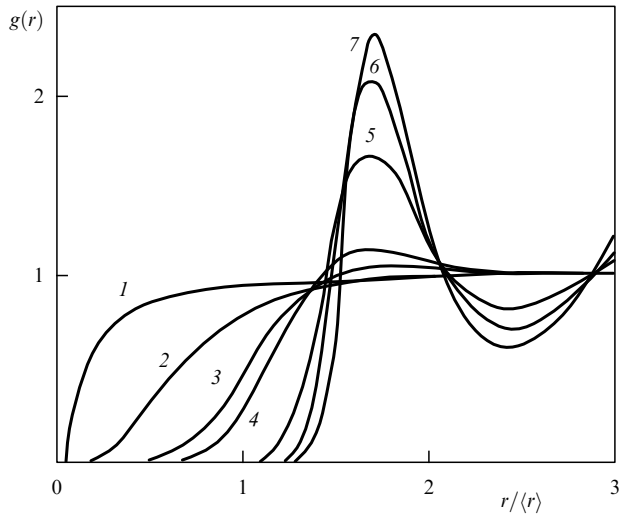

Figure 6. Pair correlation functions $g(r)$ for the one-component plasma model. Curves: *1*, $\gamma_p = 0{,}1$; *2*, $\gamma_p = 5$; *3*, $\gamma_p = 10$; *4*, $\gamma_p = 50$; *5*, $\gamma_p = 100$; *6*, $\gamma_p = 140$.

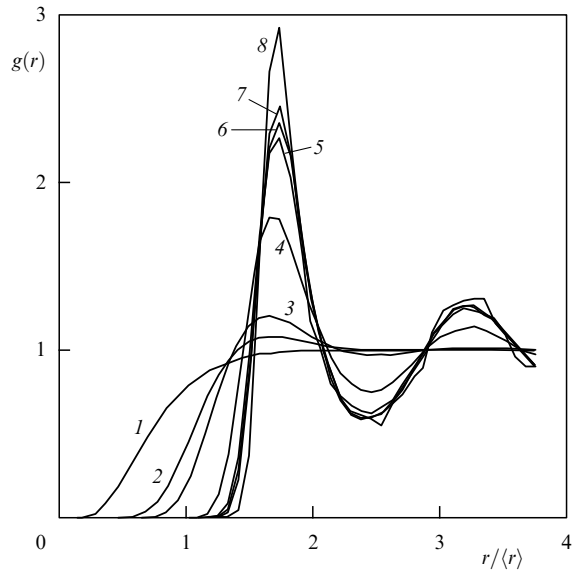

Figure 7. Pair correlation functions $g(r)$ for the Debye plasma model at $\varkappa = 1$. Curves: *1*, $\Gamma_p = 1.5$; *2*, $\Gamma_p = 7.5$; *3*, $\Gamma_p = 15$; *4*, $\Gamma_p = 75$; *5*, $\Gamma_p = 150$; *6*, $\Gamma_p = 185$; *7*, $\Gamma_p = 210$; *8*, $\Gamma_p = 1000$.

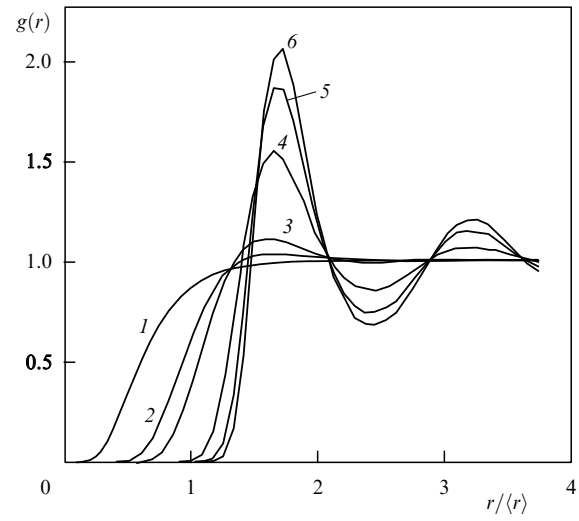

Figure 8. Pair correlation functions $g(r)$ for the Debye plasma model at $\varkappa = 2$. Curves: *1*, $\Gamma_p = 1.5$; *2*, $\Gamma_p = 7.5$; *3*, $\Gamma_p = 15$; *4*, $\Gamma_p = 75$; 5, $\Gamma_p = 150$; *6*, $\Gamma_p = 210$.

The maximum value of $S(q)$ for $\Gamma_p = 1000$ is less than 2.5, whereas [39] predicts 2.85 on the crystallization curve.

Since the analysis of spatial grain arrangement involves the use of a laser counter for measuring the correlation function, it should be remembered that the diameter of the laser beam neck is only several times less than the intergrain spacing. Therefore the method used for the diagnostics of ordered structures does not actually yield information about the correlation function itself but rather about its average over the measurement volume formed by the focusing of the laser beam. To estimate the effective dimension d_{eff} with proper account for the beam neck diameter, note that the probability of finding a particle within d_{eff} of the given particle is zero. This is true if $d_{eff} \gg D$ for non-interacting particles. Therefore d_{eff} was estimated using the experimental correlation function for CeO_2 grains in an air jet (Fig. 4a). The

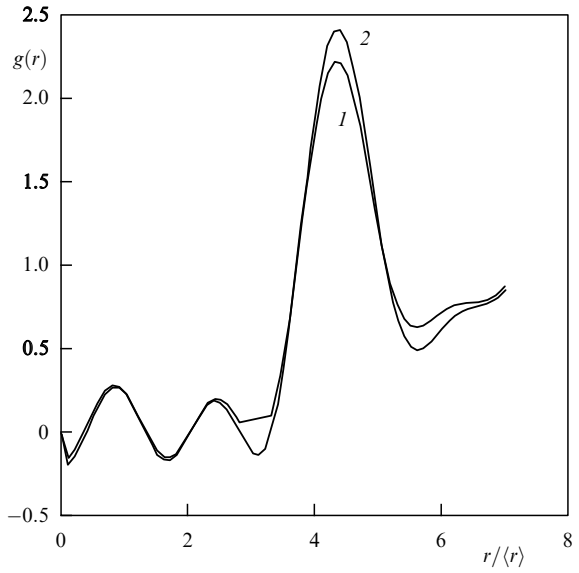

Figure 9. Structural factor for the Debye plasma model with dust grains at $\varkappa = 1$. Curves: *1*, $\Gamma_p = 216$; *2*, $\Gamma_p = 1000$.

effective dimension d_{eff} was determined from the interval within which the correlation function was zero. We estimate the dimension d_{eff} of the averaging region to be about 5 μm.

The averaged correlation functions $\langle g(r)\rangle$ are shown in Fig. 10, where the experimental pair correlation function (curve *8*) obtained under the experimental conditions described above [see Fig. 4 (curve *3*)], is also shown. Comparison of these two figures shows that the numerical results agree quite well with the experimental data. The differences, in particular the broadening of the experimental correlation function, may be due to the fact that regions of chaotically arranged grains coexist with those of ordered structures (domains). In these latter, intergrain spacings less than $\bar{r}$ are possible.

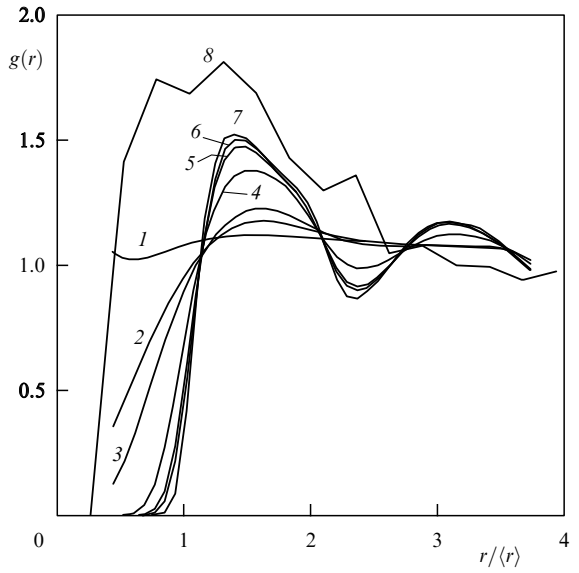

Figure 10. Averaged theoretical and experimental pair correlation functions $g(r)$ for the plasma Debye model at $\varkappa = 1$. Curves: *1*, $\Gamma_p = 1.5$; *2*, $\Gamma_p = 7.5$; *3*, $\Gamma_p = 15$; *4*, $\Gamma_p = 75$; *5*, $\Gamma_p = 150$; *6*, $\Gamma_p = 216$; *7*, $\Gamma_p = 1000$; *8*, experiment.

The existence of domains also follows from the analysis of the distributions of relative intergrain spacing $(r/\bar{r})$ for the same conditions under which the correlation functions were obtained [30]. Figures 11a and 11b show histograms for an aerosol at $T_g \cong 300$ K ('gas-like' plasma) and for a plasma at $T_g = 1700$ K. The distributions were measured for 1500–2000 particles using the time-of-flight laser counter described above and were then normalised to the area. At a plasma temperature of 1700 K the histogram becomes 4–5 times narrower and its peak shifts to small spacings ($r/\bar{r} = 0.3$) and increases in value from 6–7% to 10–11%. In this case the observed structure differs drastically from the 'gas-like' structure, thus suggesting the appearance of a strong correlation in the grain arrangement. At the same time the presence of randomly oriented grains gives rise to a broad 'gas-like' plateau on the histogram.

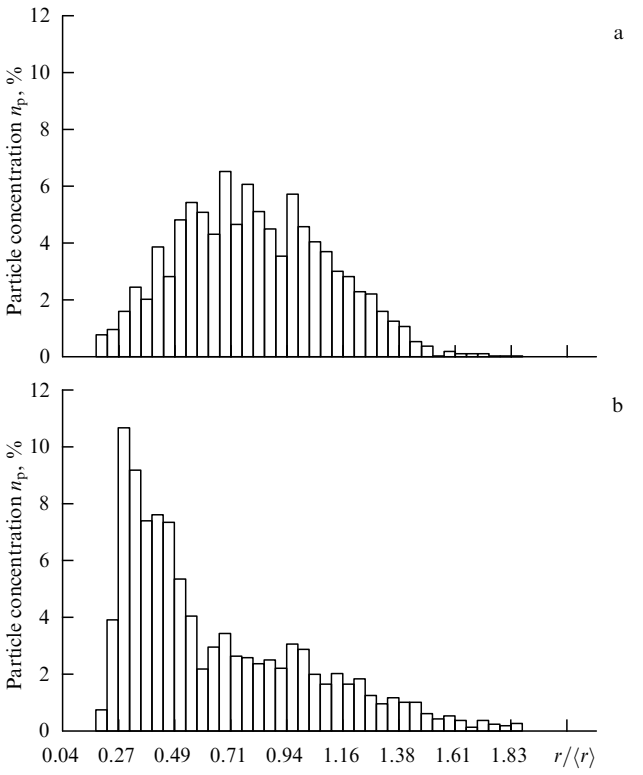

Figure 11. $r/\langle r\rangle$ distribution for CeO_2 particles in (a) an air jet at room temperature $T_g \cong 300$ K, $\gamma_p = 0$, and (b) a plasma ($Z_p = 500$) at $T_g = 1700$, $\gamma_p = 120$ ($\Gamma_s = 40$).

3. Three-dimensional structures in the positive column of a gas discharge

In contrast to thermal plasmas, a glow discharge is a non-isothermal room-temperature low-pressure plasma. Experiments were made in neon over a pressure range of 0.1 to 1.0 Torr and an electron and ion density range of 10^8 to 10^{11} cm^{-3}. The electron temperature ranged between 20 000 and 50 000 K, and the ion and atom temperature between 300 and 400 K. Under these conditions, strong fields of the stratified discharge kept particles within the volume of the plasma. Observations showed that the quasicrystalline structures, that under certain conditions develop in such a plasma, possess a number of features unknown for an RF-

discharge. Thus, these structures are essentially three-dimensional and their vertical dimension may be as great as several tens of centimeters, with an intergrain spacing ranging from 300 to 400 μm. Structure forms in the positive column far away from the electrodes, in the ionization instability region (stratum) with a relatively high degree of quasineutrality ($\sim 0.01\%$). The grain charge may reach unusually high values ($10^6 e$), which makes it possible to keep the grains in the relatively weak stratum field of order 10 V cm^{-1} (to be compared with about 100 V cm^{-1} in the near-electrode field in an RF-discharge). By varying the discharge parameters (pressure and current), dust cloud shapes in the range from nearly spherical to cylindrical can be obtained.

3.1 Experimental setup

To investigate ordered structures, a positive column of a glow discharge with natural standing strata [31] was employed. The apparatus is shown schematically in Fig. 12. The electron density, electric field, and potential in the strata show periodicity along the axis of the discharge tube [40, 41]. The particles dispersed into the column were hollow microspheres of borosilicate glass, 50 – 63 μm in diameter and 3 – 5 μm in wall thickness; and 3 – 5 μm Al_2O_3 particles.

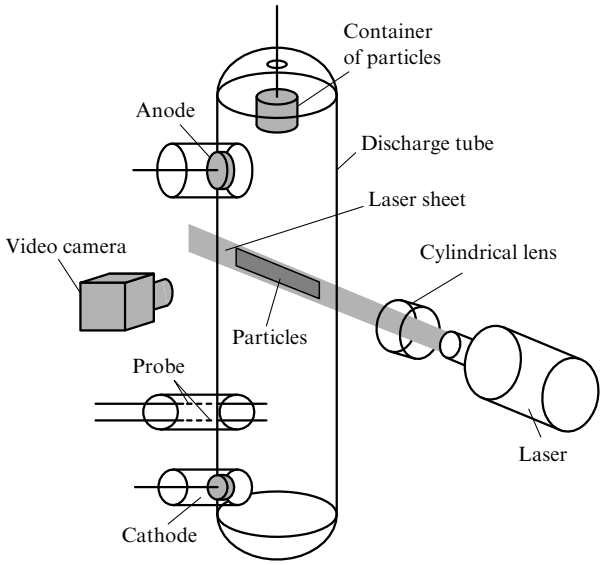

Figure 12. Outline of the experimental setup for the study of ordered structures in a gas discharge plasma.

In the presence of standing or weakly vibrating strata in the column, the particles appeared (usually) as ellipsoidal clouds in the center of their glowing regions. In a stratum region the condition of quasineutrality is obeyed to within 0.01%. Usually, there are several dust clouds located in neighboring strata several tens of centimeters away from the tube electrodes. The visualization of the particles was achieved by illuminating them with a probing argon-ion laser beam in the horizontal or vertical plane. The radiation scattered from the particles was observed with a video camera at angles of 45° and 90° for the horizontal and vertical beams, respectively. Some of the particles were also seen with the unaided eye. The signal from the camera was video recorded.

3.2 Results

The cloud diameter was 5 to 10 mm for glass microspheres and increased to 20 mm for Al_2O_3 particles. In Figures 1 and 13, typical cloud images in the vertical and horizontal planes are shown for either case. Note the ordered structure and nearly equal spacing of the grains. The image area was typically 12×17 mm in size and contained from 90 to 280 grains. In the vertical plane the grains were seen to arrange in chains.

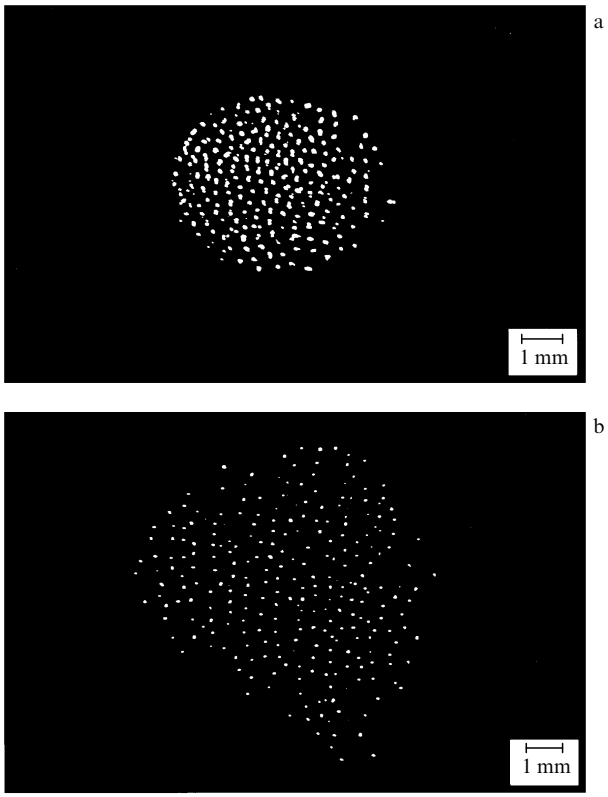

Figure 13. Video images of Al_2O_3 particles in (a) horizontal and (b) vertical planes at a discharge current of 1.15 mA and a neon pressure of 0.5 Torr; length scale 1mm.

In the elliptic case the dust grains arranged themselves in 10 – 20 (glass microspheres) and more (Al_2O_3) planar layers. The interlayer separation ranged between 250 and 400 μm and the intergrain spacing in the horizontal plane between 350 and 600 μm, corresponding to the particle densities $n_p \sim 10^3 - 10^4$ cm^{-3}. Clearly, the observed particle pattern is quasicrystalline and essentially three-dimensional in nature.

Quasicrystal formation is also borne out by the numerical analysis of the images in Figs 1 and 13. By measuring intergrain spacings, pair correlation functions were obtained. The two-dimensional correlation functions $g(r)$ for grain images in the horizontal plane are plotted in Figs 14a and 14b for glass spheres and Al_2O_3 particles, respectively. The pronounced first peak and the slow decrease of the subsequent peaks are evidence of the existence of quasicrystal structures in the plasma. The correlation length is at least four times the intergrain spacing, and the nearest neighbor distances are 400 and 500 μm for glass spheres and Al_2O_3 particles, respectively. For Al_2O_3 particles in the vertical plane, the function $g(r)$ shows damped oscillations characteristic of a liquid.

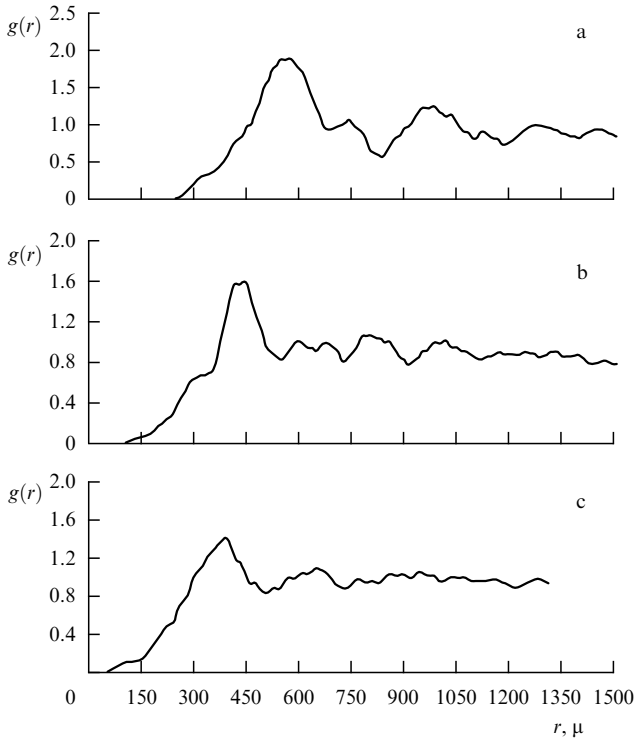

Figure 14. Pair correlation function in the (a) horizontal plane at a discharge current of 1.2 mA and a neon pressure of 0.2 Torr for glass microspheres, (b) horizontal plane at a discharge current of 1.15 mA and a neon pressure of 0.5 Torr for Al_2O_3 particles, and (c) vertical plane at a discharge current of 1.15 mA and a neon pressure of 0.5 Torr for Al_2O_3 particles. Curves a, b, and c correspond to the particle images in Figs 12a, 13b, and 13c.

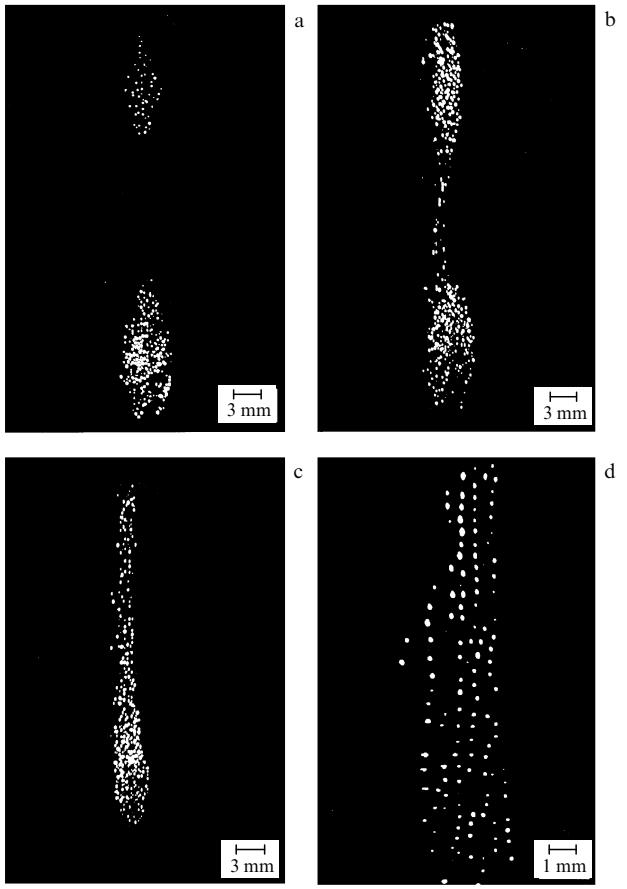

Figure 15. Video images of glass spheres in the vertical plane for various discharge current and pressure values: (a) 0.5 mA, 0.47 Torr; (b) 0.5 mA, 0.44 Torr; (c) 0.4 mA, 0.3 Torr; (d) magnified portion of the cylindrical structure shown in (b). Length scales: (a), (b), and (c), 3 mm; (d), 1mm.

Experimental data show that a stratified discharge has regions of strong and weak electric field alternating periodically along the tube axis. In the region of a strong (10 V cm^{-1}) longitudinal electric field in a stratum, a potential well arises in the vertical plane as a result of the balance of the electric and gravitational fields. A similar potential well in the horizontal plane is formed by the high (30 V) floating potential on the walls of the tube. The conclusion to be drawn from these facts is that the dust grains are kept — indeed trapped — by a strong electric field.

By varying the discharge parameters (pressure and current) it is possible to change the size of the potential well and hence the shape of the dust cloud. Reference to Figs 15a – c shows that reducing the discharge current and pressure causes two neighboring elliptic clouds to gradually transform into a cylindric shape with a vertical dimension of several tens of centimeters. In Figure 15d a magnified portion of the cylindrical structure is shown.

Varying the current may violate particle ordering thus causing the quasicrystal to 'melt'. Figure 16 shows video images of the horizontal-plane cloud of Al_2O_3 particles for three values of discharge current ($I_d = 0.4$, 0.9, and 3.85 mA) at a neon pressure of 0.3 Torr. The corresponding correlation functions are shown in Fig. 17. At $I_d = 0.4$ mA the correlation function is seen to have at least five maxima, which confirms the existence of long-range order and hence of crystalline structures in the plasma. As the current increases, both the video images and the behavior of the correlation functions indicate the violation of long-range order. At $I_d = 3.85$ mA, only short-range order is observed.

In order to estimate the coupling parameter γ_p and for comparison with numerical simulation results, the grains' kinetic energy and charge are needed. We will estimate grain parameters for typical glow discharge conditions, namely, $kT_e \approx 3$ eV, $T_i \approx 300$ K, and $n_e \sim 10^9$ cm^{-3}. In a neon discharge, grains are charged to the floating potential $V_p \sim kT_e/e \sim 3$ V. The charge on a grain is determined by the relation $Z_p = CV_p$, where C is the capacitance of the grain. For an individual sphere of radius R_p $C = R_p$, and glass microspheres 50 to 63 μm in size have a charge of the order of $10^5 e$.

The value of the charge can also be derived from the balance between the gravitational and electrical forces in a stratum, $Z_p = M_p g/eE_s$. For glass microspheres $Z_p \sim 10^6 e$ for $M_p \sim 10^{-8}$ g and $E_s \sim 10$ V cm^{-1}. This charge is about an order of magnitude greater than that obtained above for discharge parameters, the reason being that the electron energy distribution function has a second maximum at 15 eV. The grains will be charged negatively to the potential $V_p \sim kT_e/e \sim 15-30$ V in the stratum region, which is consistent with the measurement of the floating potential on the discharge tube wall in Ref. [41]. As a result, the charge is $10^6 e$ and $10^5 e$ for glass spheres and Al_2O_3 particles, respectively.

The screening (or Debye) length can be found from the balance of forces in the radial direction, $(Z_p e)\partial\varphi_D/\partial r \approx (Z_p e)E_r$, where E_r is the radial field in the discharge. For

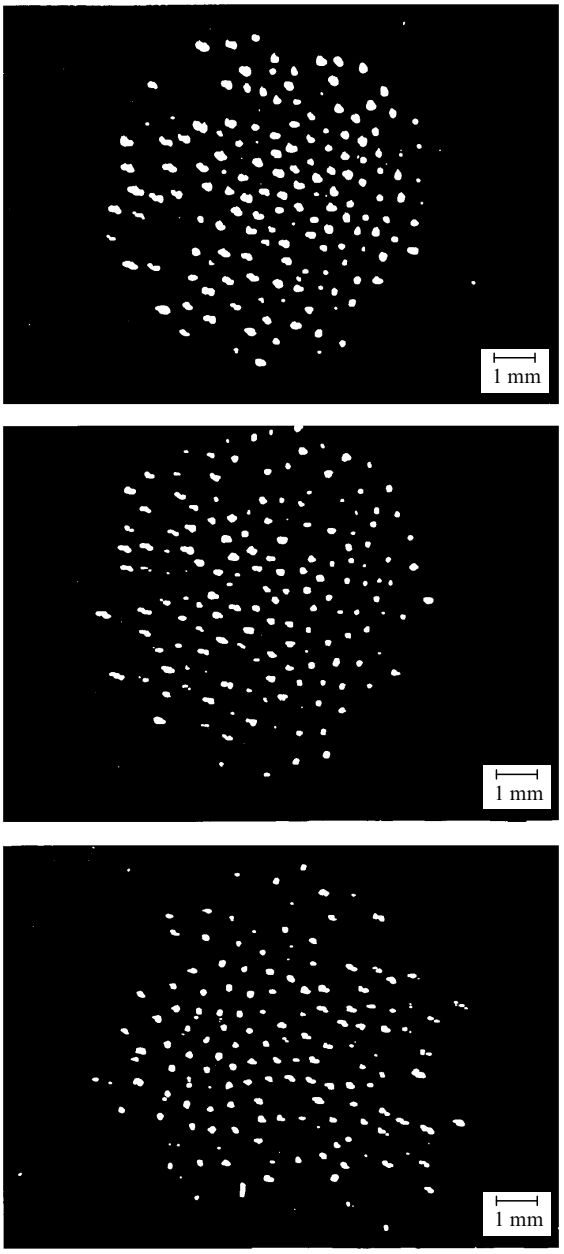

Figure 16. Video images of Al_2O_3 particles in the vertical plane for various discharge current and pressure values: (a) 0.4 mA, 0.3 Torr; (b) 0.9 mA, 0.3 Torr; (c) 3.85 mA, 0.3 Torr. Length scale 1mm.

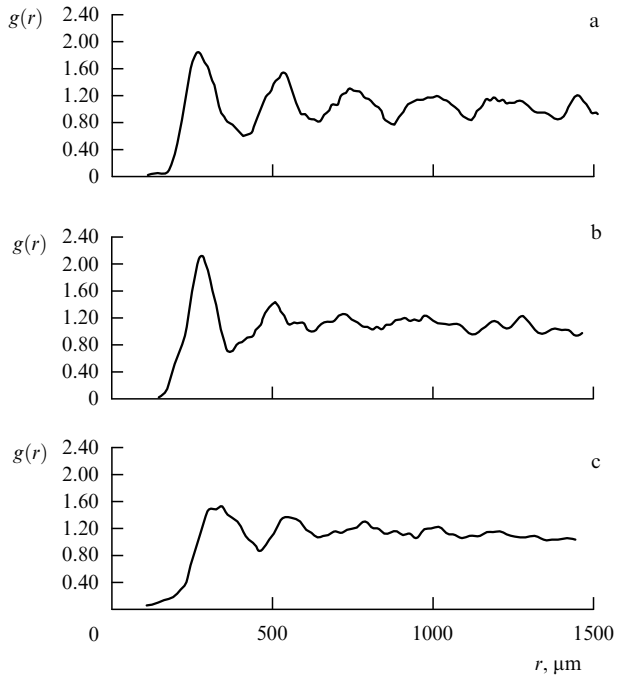

Figure 17. Vertical plane pair correlation function for (a) a discharge current of 0.4 mA and a neon pressure of 0.3 Torr, (b) a discharge current of 0.9 mA and a neon pressure of 0.3 Torr, and (c) a discharge current of 3.85 mA and a neon pressure of 0.3 Torr for Al_2O_3 particles.

typical electric fields ($E_r \sim 1$ V cm^{-1}) and intergrain spacings ($\bar{r} \approx 300-600$ μm), we find that $r_D \approx 80-100$ μm and $\bar{r}/r_D \approx 4-5$. For room temperatures, quasicrystals are found to form at coupling parameters $\gamma_p \sim 10^6$ and 10^8 for glass spheres and Al_2O_3 grains, respectively. These values are several orders of magnitude greater than those from the Debye model [21]. However, under low-pressure RF-discharge conditions the measured kinetic energy of the particles may increase to 50 eV [42]. In dc glow discharge experiments, the kinetic energy of small Al_2O_3 grains could be estimated. The video showed that the displacement of a grain from its equilibrium position is of the order of the grain diameter D_p, implying that $kT_p \sim (Z_p e)E_r D_p$. For $Z_p \sim 10^5$, $D_p \sim 5$ μm, and $E_r \sim 1$ V cm^{-1}, the coupling parameter is of the order of $\gamma_p \sim 10^3$ ($kT_p \sim 50$ eV), in fairly good agreement with the Debye model ($\gamma_p \sim 10^3$ for $\bar{r}/r_D = 4-5$).

4. UV-induced plasma

A plasma with positively charged grains can also be produced by photoemission if grains in the buffer gas are exposed to a flow of photons with energies exceeding the work function of the grain surface. Under certain conditions (size and density of the grains, wavelength and intensity of the UV radiation, and work function), crystalline structures may develop in such a system. Since the work function does not usually exceed 6 eV, photons with energy less or equal 12 eV can charge a grain without ionizing the buffer gas such as He or Ar.

Consider dust grains in a neutral gas irradiated by a UV source with a continuous spectrum, for example by a deuterium lamp with a spectral range of 200 to 300 nm. The plasma will then consist of positively charged grains and the photoelectrons they emit, both in the buffer gas which acts to cool the grains. We restrict ourselves to the case of a dilute plasma (density of neutrals $n_n \leqslant 10^{14}$ cm^{-3}), for which the photoelectron mean free path l for collisions with neutrals is much greater than the grain radius R_p ($l \gg R_p$). The positive potential of the grains is established by the balance between the electron recombination on and the photoemission current from the grain surface.

To obtain the dependence of Z_p on n_p for various dust sizes, the following values are assigned to the UV-radiation and grain parameters: grain surface temperature $T_p \approx 300$ K, the work function $\varphi_s = 1.7$ eV (typical of, for example, BaO), quantum yield $Y = 0.05$, mean quantum energy $h\nu = 2.5$ eV, and photon flux $J = 2.5 \times 10^{18}$ cm^{-2} s^{-1}, all typical deuterium lamp parameters. Following Ref. [3] it is assumed that

$T_e \approx T_{pe} \sim 0.8$ eV, which is valid if the recombination rate of electrons on the grain surface exceeds their thermal energy loss rate due to collisions with neutrals.

The variation of Z_p with n_p for the above parameters and three values of the dust grain radius ($R_p = 1$, 5, and 25 μm) are shown graphically in Fig. 18a. The decrease in the grain charge Z_p with increasing grain density n_p is explained by the fact that while the specific absorbing surface of a grain increases, the photon flux remains unchanged. Figure 18b shows the coupling parameter in the form $\gamma_p \exp(-\bar{r}/r_D)$ as a function of grain density n_p. It is seen that the condition for the crystallization of a system of dust grains, $[\gamma_p \exp(-\bar{r}/r_D) > 170]$, is satisfied for $n_p \sim 10^3$ cm^{-3}.

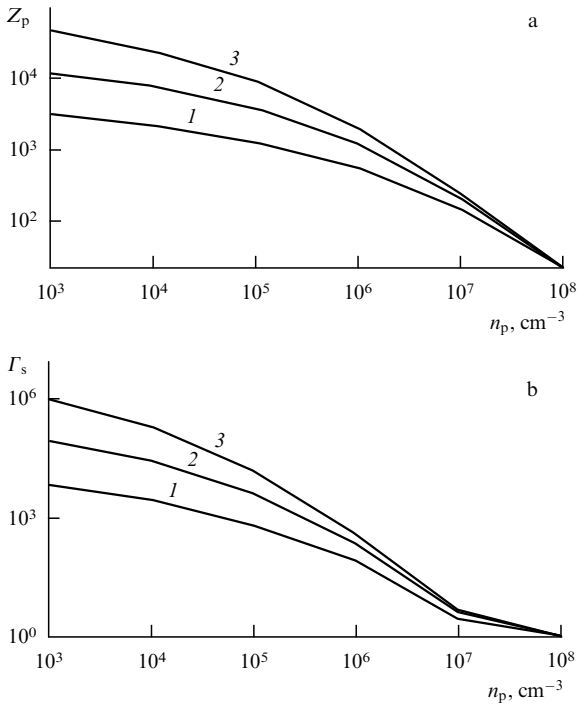

Figure 18. Grain charge Z_p (a) and interaction parameter $\Gamma_s = \gamma_p \exp(-\bar{r}/r_D)$ (b) versus density n_p for *1*, $R_p = 1$ μm; *2*, 5 μm; *3*, 25 μm.

As UV radiation is absorbed, the grains may be heated with the result that, along with photoemission, thermoelectron emission may make a noticeable contribution to the charging process. In Figures 19a and 19b, the dashed lines correspond to the thermoelectron emission from grains with a surface temperature of about 1000 K. It is seen that thermoelectron emission does not affect the formation of crystalline structures significantly.

5. Conclusions

Experiments on a thermal plasma at atmospheric pressure and on a dc glow discharge, both containing strongly coupled dust grains, have shown that for certain plasma parameters, ordered — in particular, quasicrystalline — structures of dust grains may develop under new conditions characterized by the relatively large size and essentially three-dimensional nature of the plasma and also by the fact that the formation of the structure occurs in the quasineutral bulk of the plasma rather than in its near electrode layer. The resulting ordered

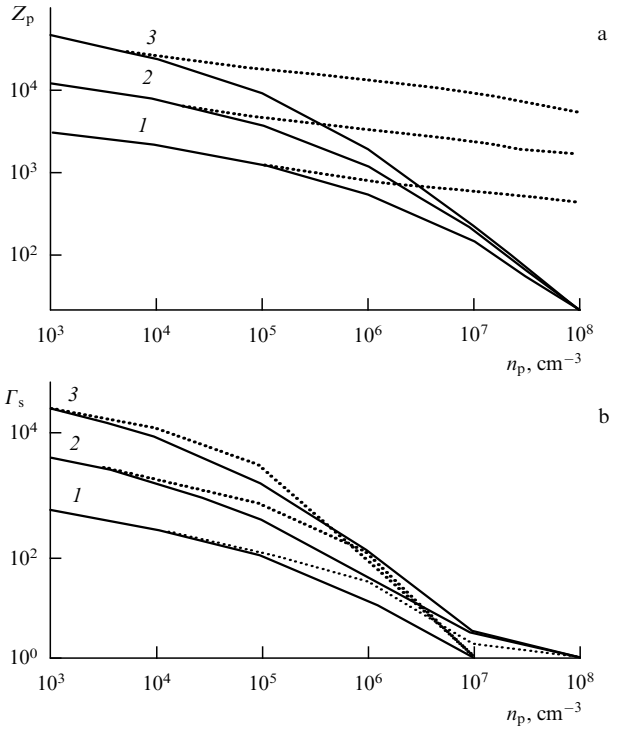

Figure 19. Grain charge Z_p (a) and interaction parameter $\Gamma_s = \gamma_p \exp(-\bar{r}/r_D)$ (b) versus density n_p for *1*, $R_p = 1$ μm; *2*, 5 μm; *3*, 25 μm, including thermoelectron emission.

structures may be adequately described by the Debye model with a screened Coulomb potential. Calculations also show that grains in a neutral buffer gas under intense UV radiation may acquire a sufficient positive charge to give rise to a crystalline structure.

As a result of the study, a number of interesting applications emerge for the crystalline structures. Dust grain structures in plasmas are a powerful tool for solving both fundamental and applied problems. Among the former are problems in plasma physics, where experiments with crystal structures are expected both to stimulate and check theoretical approaches to the modeling of strongly nonideal multicomponent plasmas. Important problem areas here are lattice defects, the thermodynamics of a lattice with and without defects, wave interaction and resonance phenomena. Results of such studies may be applied to modeling atomic and molecular crystals (solid state physics). The study of phase transitions in dust grain systems (including their multiparticle self-organization) may contribute insight into the condensation process (critical phenomena). The possibility of manufacturing small systems of only a few dust grains is important in that the study of their chaotic motion and of their response to external fields will provide a better understanding of dynamical processes in such systems. On the application side, microelectronics uses, in particular those for the removal of particles in microchip manufacturing and for the modeling of small crystals (nanocrystals) in plasma evaporation, are to be noted.

References

1. Sodha M S, Guha S *Adv. Plasma Phys.* **4** 219 (1971)
2. Fortov V E, Yakubov I T *Neideal'naya Plazma* (Nonideal Plasma) (Moscow: Energoatomizdat, 1994) p. 282
3. Rosenberg M, Mendis D A *IEEE Trans. Plasma Sci.* **23** 177 (1995)

4. Sugden T M, Thrush B A *Nature* (London) **168** 703 (1951)
5. Shuler K E, Weber J *J. Chem. Phys.* **22** 491 (1954)
6. Bouchoule A, Boufendi L *Plasma Sources Sci. Technol.* **3** 292 (1994)
7. Goree J *Plasma Sources Sci. Technol.* **3** 400 (1994)
8. Ichimaru S *Rev. Mod. Phys.* **54** 1017 (1982)
9. Ikezi H *Phys. Fluids* **29** 1764 (1986)
10. Fortov V E et al. *Phys. Lett. A* **229** 317 (1997)
11. Wuerker R F, Shelton H, Langmuir R V *J. Appl. Phys.* **30** 342 (1959)
12. Gilbert S L, Bollinger J J, Wineland D J *Phys. Rev. Lett.* **60** 2022 (1988)
13. Chu J H, Lin I *Phys. Rev. Lett.* **72** 4009 (1994)
14. Thomas H et al. *Phys. Rev. Lett.* **73** 652 (1994)
15. Hayashi Y, Tachibana K *Jpn. J. Appl. Phys.* **33** L804 (1994)
16. Melzer A, Trottenberg T, Piel A *Phys. Lett. A* **191** 301 (1994)
17. Raizer Yu P, Shneider M N, Yatsenko N A *Vysokochastotnyĭ Ёmkostnyĭ Razryad* (High Frequency Capacitance Discharge) (Moscow: MFTI; Nauka, 1995)
18. Trottenberg T, Melzer A, Piel A *Plasma Sources Sci. Technol.* **4** 450 (1995)
19. Morfill G E, Thomas H *J. Vac. Sci. Technol. A* **14** 490 (1996)
20. Slattery W L, Doolen G D, DeWitt H E *Phys. Rev. A* **21** 2087 (1980)
21. Robbins M O, Kremer K, Grest G S *J. Chem. Phys.* **88** 3286 (1988)
22. Stevens M J, Robbins M O *J. Chem. Phys.* **98** 2319 (1992)
23. Farouki R T, Hamaguchi S *Appl. Phys. Lett.* **61** 2973 (1992)
24. Rahman A, Schiffer J P *Phys. Rev. Lett.* **57** 1133 (1986)
25. Dubin D H E, O'Neil T M *Phys. Rev. Lett.* **60** 511 (1988)
26. Fortov V E et al. *Pis'ma Zh. Eksp. Teor. Fiz.* **63** 176 (1996) [*JETP Lett.* **63** 187 (1996)]
27. Fortov V E et al. *Pis'ma Zh. Eksp. Teor. Fiz.* **64** 86 (1996) [*JETP Lett.* **64** 92 (1996)]
28. Raizer Yu P *Fizika Gazovogo Razryada* (Gas Discharge Physics) (Moscow: Nauka, 1987) [Translated into English (Berlin, New York: Springer Verlag, 1997)]
29. Kondrat'ev A B et al. *Teplofiz. Vys. Temp.* **32** 452 (1994) [*High Temp.* **32** 452 (1994)]
30. Fortov V E et al. *Phys. Lett. A* **219** 89 (1996)
31. Fortov V E et al. *Zh. Eksp. Teor. Fiz.* **111** 889 (1997) [*Sov. Phys. JETP* **84** 489 (1997)]
32. Fomenko B S *Émissionnye Svoĭstva Materialov* (Emission Properties of Materials) (Kiev: Naukova Dumka, 1981) p. 164
33. Kosov V F, Molotkov V I, Nefedov A P *Teplofiz. Vys. Temp.* **29** 633 (1991)
34. Benilov M S *Teplofiz. Vys. Temp.* **26** 993 (1988) [*High Temp.* **26** 780 (1988)]
35. Nefedov A P, Petrov O F, Vaulina O S to be published *Appl. Opt.* (1997)
36. Fortov V E et al. *Phys. Rev. E* **54** R2236 (1996)
37. Zamalin V M, Norman G E, Filinov V S *Metod Monte-Carlo v Statisticheskoĭ Termodinamike* (Monte Carlo Method in Statistical Physics) (Moscow: Nauka, 1977)
38. Sood A K *Solid State Phys.* **45** 1 (1991)
39. Hansen J P, Verlet L *Phys. Rev.* **184** 151 (1969)
40. Golubovskiĭ Yu B, Nisimov S U, Suleimenov I E *Zh. Tekh. Fiz.* **64** 54 (1994) [*Tech. Phys.* **39** 1005 (1994)]
41. Golubovskiĭ Yu B, Nisimov S U *Zh. Tekh. Fiz.* **65** 46 (1995) [*Tech. Phys.* **40** 24 (1995)]